TOP-DOWN ESTIMATE OF METHANE EMISSIONS IN CALIFORNIA USING A MESOSCALE INVERSE MODELING TECHNIQUE

Yu Yan Cui*, Jerome Brioude, Gregory J. Frost, Jeff Peischl
Chemical Sciences Division, Earth System Research Laboratory, NOAA, Boulder
Cooperative Institute for Research in Environmental Sciences, University of Colorado, Boulder

Thomas Ryerson, Michael Trainer
Chemical Sciences Division, Earth System Research Laboratory, NOAA, Boulder

Steve C. Wofsy, Gregory W. Santoni
Department of Earth and Planetary Sciences, Harvard University, Cambridge

Eric Kort
Department of Atmospheric, Oceanic and Space Sciences, University of Michigan, Ann Arbor

1. INTRODUCTION

The atmospheric mixing ratio of the greenhouse gas methane (CH_4) has tripled in the last 200 years, having been nearly constant for the previous 1⁄2 million (Hansen et al. 2006, IPCC 2007). Reducing emissions of methane may be an important component of an initial strategy for avoiding the most severe impacts of global warming (Wennberg et al. 2012, Brandt et al. 2014). Recently, many studies found there were clear discrepancies in CH_4 emissions inventories derived between the "bottom-up" and the "top-down" methods, which is strangling government regulations and further greenhouse gases studies in air quality, energy, ecosystem and climate.

Current "top-down" atmospheric studies have shown that CH_4 were underestimated in the United States by official inventories (Kort et al. 2008, Miller et al. 2013, Brandt et al. 2014), especially for south-central US and California. The Inventory of greenhouse gases in California has been enforced by the legislature to update every five years in term of Assembly Bill 32 of 2006, which enacted into law as the California Global Warming Solutions Act and required statewide greenhouse gas emissions not to exceed 1990 levels by the year 2020. Therefore, studies have focused on the updates in CH_4 emission inventories in California, such as the South Coast Air Basin (SoCAB) and the California's Central Valley. The SoCAB is a primary coastal urban region (Los Angeles metropolitan region) contributing CH_4 emissions to the statewide (Peischl et al. 2013, Wecht et al. 2014), which natural gas emissions were found should be higher than current official inventories. "Top-down" studies have estimated CH_4 emissions in this area based on a ground-based Fourier transform spectrometer (FTS) (Wunch et al. 2009), airborne measurements (Perschl et al. 2013), and satellite observations (Wecht et al. 2014). All of them show a factor of ~two higher emissions than the "bottom-up" inventories.

The Central Valley is another primary sources for CH_4 emissions to the statewide (Zhao et al. 2009, Jeong et al. 2013) such as contributions from livestock, rice paddies, and natural gas emissions. Sacramento Valley and San Joaquin Valley compose the Central Valley. Rice cultivation was underestimated by current official statewide inventory in the Sacramento Valley (Peischl et al. 2012), and due to complex terrains inducing complex meteorology regionally and locally in the San Joaquin Valley (Zhong et al. 2004), there were inadequate studies to constrain and quantify the surface CH_4 emissions in this area.

2. METHODS

2.1 Observations and Prior inventory

CalNex campaign (Ryerson et al. 2013) is a good opportunity to expand the estimation and evaluation of CH_4 emission inventories in California taking advantages in spatial coverage by the NOAA P-3 aircrafts. In context of CalNex field intensives, we used six flights measurements (May 5, May 8, May 14, May 16, May 19 and June 20) for the inversed CH4 emissions in the SoCAB

**Corresponding author:* Yuyan Cui, Chemical Sciences Division, Earth System Research Laboratory, NOAA, Boulder, Room 2A105, 325 Broadway, Boulder, CO, 80305; e-mail: Yuyan.Cui@noaa.gov

and seven flights measurements (May 7, May 11, May 12, May 24, June 14, June 16, and June 18) for the Central Valley. All of these were flights dedicated to characterizing daytime (late morning and afternoon after vertical mixing) emissions and chemistry in the two areas. Only the observations in the boundary layer were used in the inversions (Brioude et al. 2013a). Technique details in measurements of CH_4 on the research aircraft are shown in Peischl et al., (2012, 2013). The measurements in the SoCAB and the Central Valley were not far from the surface sources, and hence secondary production of CH_4 can be neglected. Meanwhile, we did not consider soil sink for CH_4 lifetime in the atmosphere and assume CH_4 are passive tracers throughout the paper, regardless of the position of the measurements relative to the sources (Brioude et al. 2013a).

The 4 × 4 km EPA NEI05 (US Environmental Protection Agency, 2010) is used (Brioude et al. 2011) as the prior emission estimate for the optimization of CH_4 surface emission inventories. In the study, the CH_4 posterior estimates are compared with the NEI 2005 emission estimates.

2.2 FLEXPART-WRF

To simulate the atmospheric transport at mesoscale, we used Weather Research and Forecasting (WRF) mesoscale research model as input to drive FLEXPART (FLEXPART-WRF) with back-trajectories mode to estimate CH_4 emissions. We used three different WRF configurations to represent three different transport models. For the three WRF configurations, the first two have been evaluated and did fairly well performances for scientific studies in the California area and the third one is a new configuration and the publication is preparing by Kim et al. (2015). The first one we used is from "EM4N" configuration of Angevine et al. (2012, 2013) ("wa"). The second one we used is from WRF-Chem 3.1 configuration of Kim et al. (2011) ("sw_old"). And the third one we used is WRF-Chem 3.4 with nested grids at 12 and 4 km spacing with 60 vertical levels ("sw_new"). GFS FNL data were used as a global model meteorological initial and boundary condition. The Noah land surface model and the YSU boundary layer scheme were used.

FLEXPART-WRF version 3.1 (Stohl et al., 2005, Brioude et al. 2013b) is used to simulate atmospheric transport. A total of 10,000 back trajectories were released every 30 s or every 100 m during vertical profiles along the aircraft flight tracks. FLEXPART simulated the trajectories over 24 h to focus on the local transport. Here we assume all emissions occur within a surface layer of 100 m depth in our FLEXPART back trajectories. Here the FLEXPART output had a resolution of 8 × 8 km, and the output consists of a residence time in the surface layer weighted by the atmospheric density. When this output is combined with a surface flux emission inventory, one can calculate a mixing ratio for each set of trajectories along the aircraft flight track. In this way, FLEXPART linearizes the transport processes between the surface and the aircraft, so that an adjoint model of WRF-Chem is unnecessary to apply an inverse modeling technique (de Foy et al. 2012, Brioude et al. 2013a, de Foy et al. 2014).

2.3 Inverse modeling

An inverse modeling approach used here is developed based on Brioude et al. (2011). The observations in the inverse modeling are CH_4 enhancements, calculated by subtracting the modeled background from the flight observations. We defined the chemical background of CH_4 as the lowest mixing ratio found in the atmospheric boundary layer (< 2km) upwind of the study areas. The enhancements of CH4 are ~10% of background concentrations. Uncertainties arising from the background definitions were added to the measurement uncertainties in the inversion. To calculate the best estimates of CH_4 surface flux emissions, we used a lognormal cost function in a 4-dimensional (4-D = 3 spatial dimensions plus time) least squares method. The advantage of using a lognormal cost function is that no negative fluxes are found in the posterior.

We used a Bayesian least squares method to invert the observed concentrations and determine the surface fluxes. The covariance matrix of the observations includes uncertainties from the measurements and the background definition for each flight and is assumed to be diagonal. The observation error is assumed to be uncorrelated. The covariance matrices of the observation and prior estimate are not perfectly known, and therefore uncertainties in the posterior can arise from the assumptions made about those covariance matrices. To overcome this issue, we used the L-shape criterion method to balance the errors in both covariance matrices to obtain a posterior estimate with the smallest sensitivity to the error in either the observation or prior covariance matrices (Henze et al., 2009).

We included 4 time steps in the 4-D inversion: one time step between 13:00 and 17:00 UTC that

includes the morning rush hour, a time step between 17:00 and 21:00 UTC to represent midday conditions, a time step between 21:00 UTC to 01:00 UTC that includes the evening rush hour, and a time step between 01:00-13:00 UTC representing the nighttime emissions. These time steps were chosen based on the overall week diurnal cycle in the NEI05 for the SoCAB, and the temporal distribution of the aircraft observations during CalNex, which occurred between 16:00 UTC and 01:00 UTC. The values reported in the results section are the averages for the two time steps between 17:00 UTC and 01:00 UTC where we have the strongest confidence in the transport models and therefore in the inversion.

In this study, in order to eliminate the cross-correlations for low values of emissions and also efficiently obtain inversion solutions, we clustered spatial grids in study areas using an optimality criteria based on the Fisher information matrix. Here we used a similar criterion (eq 1) as Bocquet el al. (2011) to construct adaptive grids of the control space.

$$\mathcal{J} = \mathrm{Tr}(\mathrm{BW^T R^{-1} W}) \qquad (1)$$

$\mathcal{J}$ is the criterion. B is the covariance matrix of the prior emission inventory, R is the covariance matrix of the measured observation and the simulated concentrations by a model H, and W is the derivative of the model H assuming lognormal distribution. Using the control space we classified them into clusters according to the principle of neighbor method, that is if the grid and its four neighbors (up, down, left, and right) has similar values, they are aggregated as a cluster. In addition, for high scores in the control space, we keep each grid as a cluster. We reduced the total grids in the inverse system by a factor of ~5, and saved computation time without loosing information contrary to other methods (e.g. Brioude et al., 2013a).

3. RESULTS AND DISCUSSION

The aforementioned methods are applied to the SoCAB and Central Valley regions. Results from the SoCAB analysis are presented here.

3.1 Emission strength

The inverse system constrained the emissions of CH_4 (posterior inventory) using the transport model to better match the aircraft observations in the time series of CH_4 mixing ratio. Fig 1 shows comparisons between observations and simulations in time series of CH_4 mixing ratio based on six flight measurements. With the same transport model, the inventory optimized by this study (posterior inventory) simulated higher agreements with observations, comparing the results with the inventory originated from NEI05 (prior inventory). The R^2 correlation between observations and inversion results in time series of CH4 mixing ratio for each flight with each transport model are estimated as well (not shown here). R^2 correlation was improved using the inverse system with value of ~0.7 compared ~0.5 using prior inventory.

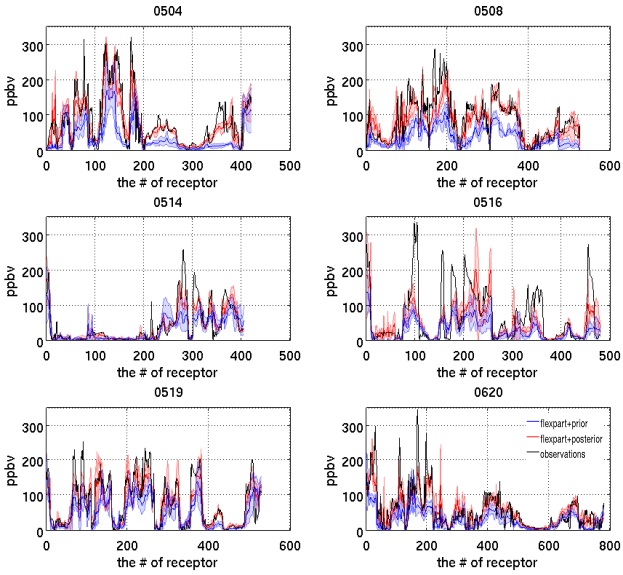

Fig 1. The comparison of observations and models in time series of the CH_4 concentration for flights 0504, 0508, 0514, 0516, 0519, and 0620, which flew over the SoCAB. The shaded areas indicate 1σ variability for three WRF configurations.

The values from the posterior inventory calculated by the inverse model are shown in Fig 2 based on each flight over the SoCAB and each transport model, respectively. The median values from "wa" transport model show variation range between 300 to 600 Gg CH_4/yr with uncertainty between 9% and 19%, from "sw_old" show variation range between 350 to 550 Gg CH_4/yr with uncertainty between 10% and 15%, and from "sw_old" show variation range between 350 to 500 Gg CH_4/yr with uncertainty between 11% and 15%. The mean values of six flights based on each transport model are shown in Fig 2 as well. Three transport models show similar median values ~420 Gg CH_4/yr from the six flights with uncertainty of 28%, 18%, and 18% respectively. "wa" show relatively higher variations than others.

Combining the three transport models, we estimated an optimized value of 426$\pm$ 93 Gg CH_4/yr for the SoCAB area (Fig 3), in the range of previous studies relating to the time period of

CalNex campaign (440±100 Gg CH_4/yr (Wennberg et al. 2012), 410±40 Gg CH_4/yr (Peischl et al. 2013), 280-390 Gg CH_4/yr (Santoni et al. 2014), and 420±80 Gg CH_4/yr (Wecht et al. 2014)). Here we estimated that this robust evaluation is higher by factor of ~2 than NEI 2005 (230 Gg CH_4/yr) with 15 % uncertainty.

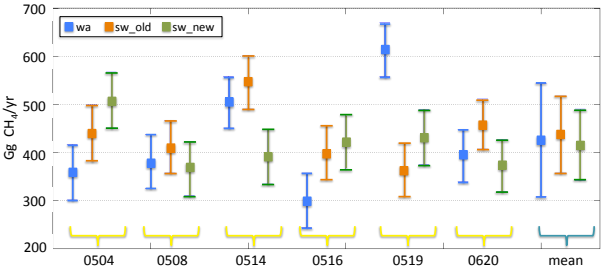

Fig 2. Daytime averaged annual total emissions of CH4 (Gg/yr) derived based on each of flights flew over the SoCAB area, and each transport model. The mean values are calculated based on each transport model as well.

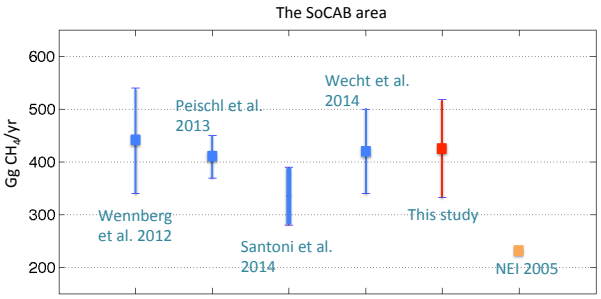

Fig 3. Previous studies for total emissions of CH4 in the SoCAB relating to the CalNex campaign, the estimates from this study, and the value form prior inventory.

3.2 Spatial Distribution

The surface emissions of CO have been improved by Brioude et al. (2013) in the similar inverse system. Ratios of CH_4 and CO from six flights (over the SoCAB) are shown in Fig 4, including observations, estimates from prior inventories of CH_4 and CO, and estimates from posterior inventories of CH_4 and CO. Ratios of CH_4 and CO based on prior inventories show underestimates compared with observations. The distinct improvements are shown in ratios of CH_4 and CO based on the posterior inventories of this study, which implies the improvement of CH_4 in spatial distributions from the posterior inventory.

Fig 5 displays the spatial distribution of four main source types attributed to emissions of CH_4 in the SoCAB area with 8km spatial resolution from NEI 2005. The four sources include dairy, landfill, wells, and point sources. Dairy CH_4

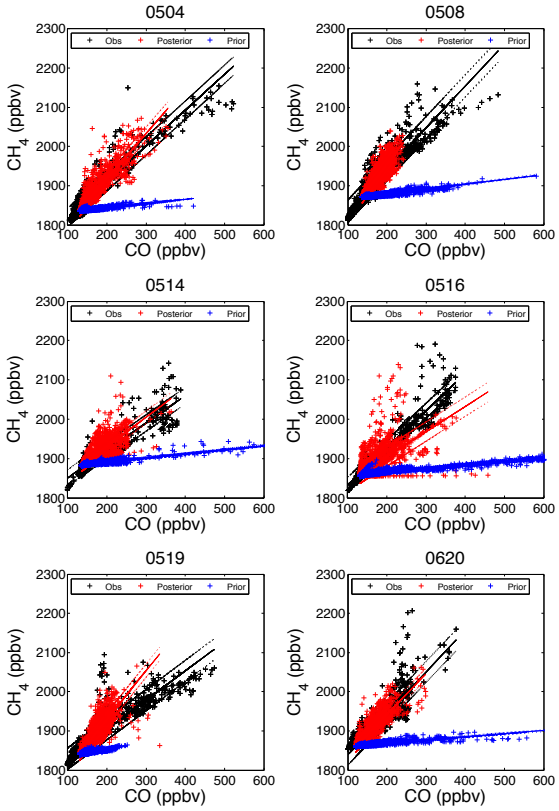

Fig 4. The comparison of measurements and simulations in the ratio between CH_4 and CO for cases of flights 0504, 0508, 0514, 0516, 0519, and 0620. Here results include three WRF configurations. The dash lines represent estimates in one standard deviation.

emissions predominate in the eastern basin of the SoCAB, and CH_4 emissions of well, landfill, and point sources dominate in the western basin. It is clear that the emission strength of point sources is lower than dairy and landfill sources. CH_4 emissions from Landfill are also distributed in the eastern basin. We check the overlap grids between the four sources, and found the number of overlap grids between the dairy sources and other three sources are small, and other sources in these overlap grids show very small emission values (~ 2 order smaller) compared with others in non-overlap grids. Therefore, we consider dairy sources total contributed the CH_4 emissions in the grids in Fig 5 (first panel). However, we cannot differentiate the overlap grids between well, landfill, and point sources here. Therefore, we estimated CH_4 emissions of dairy source between the prior and posterior inventories, and we

estimated total CH_4 emissions of three sources together (well, landfill, and point sources) between the prior and posterior inventories. We assume the spatial distributions of source types are correct.

Fig 6 shows spatial distribution of CH_4 and CO emissions in prior and posterior inventories, and also the ratio of CH_4 and CO in spatial distributions. The comparisons of ratios of CH_4 and CO calculated from prior inventories (NEI05) and ratios of CH_4 and CO calculated from this study clear show differences in spatial distributions. Consistent with results of CO posterior inventory in Brioude et al. (2013), we Found in Fig 6 (f), ratios of CH_4 and CO emphasized the enhancements in the landfill, wells and point sources, especially for the western basin.

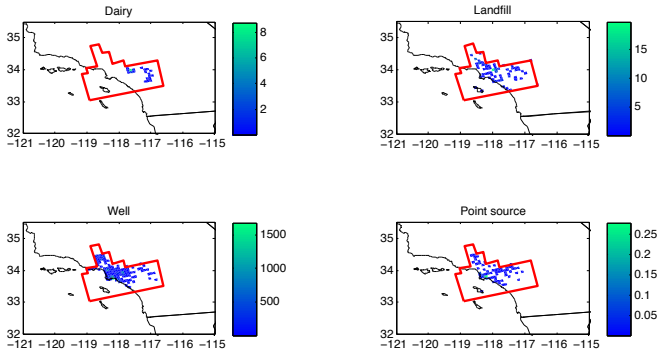

Fig 5. CH_4 emissions by source types from NEI05 for the SoCAB domain, including four sectors: diary, landfill, well, and point source of CH4. The units for diary, landfill, and point sources are Gg CH_4/yr per grid cell, and the unit of well source is #well per grid cell.

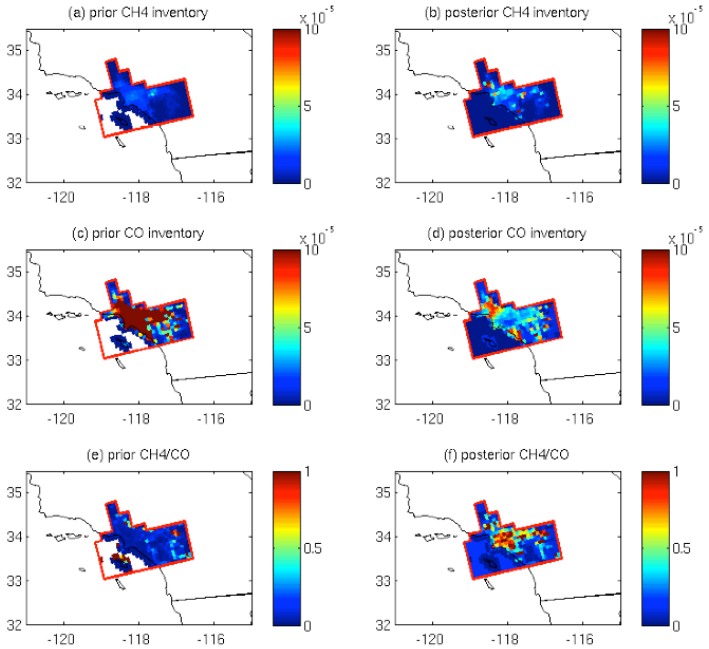

Fig 6. Surface CH_4 emissions in prior inventory (a) and posterior inventory (b), surface CO emissions in prior inventory (c) and posterior inventory (d), with unit: mole m^{-2} s^{-1} , and the ratios of CH_4 and CO in prior inventory (e) and posterior inventory (f).

4. CONCLUSION

Here we applied an inverse modeling technique using three mesoscale transport models and in situ measurements from the NOAA P-3 aircraft during the 2010 CalNex campaign over the SoCAB to evaluate and improve the NEI 2005 emission inventory of CH_4. We based on the receptor-oriented framework to provide robust validation the NEI05 emission inventory of CH_4. Aggregating grids to clusters is new to our inverse modeling technique. The inversions were applied to individual flights' data with three different transport models, respectively. The uncertainty of the average flux in the SoCAB from these single flight inversions was about 15 % for CH_4 emissions. Compared to NEI 2005, the daytime CH_4 posterior estimates were higher by factor of two in the SoCAB, which is in agreement with a recent study based on observations. The posterior inventory using the mesoscale inverse technique here also provide more details of the regional spatial distribution in CH_4 emissions which supplement and enhance our understanding in statewide emissions of CH_4.

Therefore, we use the inverse model to study emissions of CH_4 in the Central Valley. We found there was three times higher in our top-down method in total CH_4 emissions for the Central Valley than values from EPA NEI 2005. We also estimate spatial distributions of CH_4 surface fluxes and discuss the significant role of dairy, rice and well sources that contributed to the discrepancies between our top-down calculations and bottom-up inventories.

5. REFERENCES

Angevine, W. M., L. Eddington, K. Durkee, C. Fairall, L. Bianco, and J. Brioude, 2012: Meteorological model evaluation for calnex 2010, *Mon. Wea. Rev.* , **140**, 3885–3906.

Bao, J. W., S. A. Michelson, P. O. G. Persson, I. V. Djalalova, and J. M. Wilczak, 2008: Observed and wrf-simulated low- level winds in a high-ozone episode during the central california ozone study, *J. Appl. Meteor. Climatol.*, **47**, 2372–2394.

Bocquet, M., L. Wu, and F. Chevallier, 2011: Bayesian design of control space for optimal assimilation of observations. part I: Consistent multiscale formalism, *Q J Roy Meteor Soc*, **137**, 1340–1356.

Brandt, A. R., et al., 2014: Methane leaks from north amer- ican natural gas systems, *Science*, **343**, 733–735.

Brioude, J., et al., 2011: Top-down estimate of anthropogenic emission inventories and their interannual variability in Houston using a mesoscale inverse modeling technique, *J Geophy Res-Atmos*, **116**, doi:10.1029/2011jd016215.

Brioude, J., W. M. Angevine, S. A. McKeen, and E. Y. Hsie, 2012: Numerical uncertainty at mesoscale in a lagrangian model in complex terrain, *Geoscientific Model Develop.*, **5**, 1127–1136.

Brioude, J., et al., 2013a: Top-down estimate of surface flux in the los angeles basin using a mesoscale inverse modeling technique: assessing anthropogenic emissions of CO, NOx and CO2 and their impacts, *Atmos. Chem. Phys.*, **13**, 3661–3677.

Brioude, J., et al., 2013b: The lagrangian particle dispersion model Flexpart-Wrf version 3.1, *Geoscientific Model Develop.*, **6**, 1889–1904.

de Foy, B., C. Wiedinmyer, and J. J. Schauer, 2012: Estimation of mercury emissions from forest fires, lakes, regional and local sources using measurements in Milwaukee and an inverse method, *Atmos. Chem. Phys.*, **12**, 8993– 9011.

de Foy, B., J. Heo, and J. J. Schauer, 2014: Estimation of direct emissions and atmospheric processing of reactive mercury using inverse modeling, *Atmos. Environ.,* **85**, 73–82.

EPA (2011). Inventory of US Greenhouse Gas Emissions and Sinks: 1990-2009, USEPA #430-R-11-005.

Hansen, J., M. Sato, R. Ruedy, K. Lo, D.W. Lea, and M. Medina-Elizade, 2006: Global temperature change. *Proc. Natl. Acad. Sci.*, **103**, 14288-14293.

Henze, D.K., J.H. Seinfeld, and D.T. Shindell, 2009: Inverse modeling and mapping US air quality influences of inorganic PM2.5precursor emissions using the adjoint of GEOS-Chem. *Atmos. Chem. Phys.*, **9**, 5877-5903.

IPCC Fourth Assessment Report: Climate Change 2007 (AR4)

Jeong, S., Y.-K. Hsu, A. E. Andrews, L. Bianco, P. Vaca, J. M. Wilczak, and M. L. Fischer, 2013: A multi-tower measurement network estimate of California's methane emissions, *J Geophys Res-Atmos*, **118**, 11,339–11,351.

Kort, E. A., et al., 2008: Emissions of CH_4 and N_2O over the united states and Canada based on a receptor-oriented modeling framework and COBRA-NA atmospheric observations, *Geophys Res Lett*, **35**, doi:10.1029/2008gl034031.

Miller, S. M., et al., 2013: Anthropogenic emissions of methane in the united states, *Proc. Natl. Acad. Sci.,* **110**, 20,018– 20,022.

Peischl, J., et al., 2012: Airborne observations of methane emissions from rice cultivation in the Sacramento valley of California, *J Geophys Res-Atmos*, **117**, doi: 10.1029/2012jd017994.

Peischl, J., et al., 2013: Quantifying sources of methane using light alkanes in the Los Angeles basin, california, *J Geophys Res-Atmos*, **118**, 4974–4990.

Ryerson, T. B., et al., 2013: The 2010 California research at the nexus of air quality and climate change (CalNex) field study, *J Geophys Res-Atmos*, **118**, 5830–5866.

Wecht, K. J., Jacob, D. J., Sulprizio, M. P., Santoni, G. W., Wofsy, S. C., Parker, R., Bösch, H., and Worden, J. 2014: Spatially resolving methane emissions in California: constraints from the CalNex aircraft campaign and from present (GOSAT, TES) and future (TROPOMI, geostationary) satellite observations, *Atmos. Chem. Phys.,* **14**, 8173-8184.

Wennberg, P. O., et al., 2012: On the sources of methane to the Los Angeles atmosphere, *Environ Sci Technol*, **46**, 9282–9289.

Wunch, D., P. O. Wennberg, G. C. Toon, G. Keppel-Aleks, and Y. G. Yavin (2009), Emissions of greenhouse gases from a north american megacity, *Geophys Res Lett*, **36**, doi:10.1029/2009gl039825.

Zhao, C., A. E. Andrews, L. Bianco, J. Eluszkiewicz, A. Hirsch, C. MacDonald, T. Nehrkorn, and M. L. Fischer, 2009: Atmospheric inverse estimates of methane emissions from Central California, *J Geophys Res-Atmos*, **114**, doi:10.1029/2008jd011671.

Zhong, S. Y., C. D. Whiteman, and X. D. Bian, 2004: Diurnal evolution of three-dimensional wind and temperature structure in California's central valley, *J Appl. Meteor.*, **43**, 1679–1699, doi:10.1175/jam2154.1.